Effect of Biological Control Antagonists Adsorbed on Chitosan Immobilized Silica Nanocomposite on *Ralstonia solanacearum* and Growth of Tomato Seedlings

Gatahi Dennis[1], Wanyika Harrison[2*], Kihurani Agnes[3] and Gatebe Erastus[4]

[1]*Department of Horticulture, Jomo Kenyatta University of Agriculture and Technology, P.O.Box 62000-00200, Nairobi, Kenya.*
[2]*Department of Chemistry, Jomo Kenyatta University of Agriculture and Technology, P.O.Box 62000-00200, Nairobi, Kenya.*
[3]*Department of Crop Science, Karatina University, P.O.Box 1957-10101, Karatina, Kenya.*
[4]*Kenya Industrial Research and Development Institute, P.O.Box 30650-00100, Nairobi, Kenya.*

Authors' contributions

This work was carried out in collaboration between all authors. Author WH designed the study, sourced the materials and supervised the experiments. Author KA managed all literature searches, supervised the experiments and validated the protocols. Author GE approved the manuscripts. Author GD performed the experiments, wrote the protocols and wrote the first draft of the manuscript. All authors read and approved the final manuscript.

Article Information

Original Research Article

ABSTRACT

Background: Biological control holds promise in managing bacterial wilt disease. However, its efficacy is limited by harsh environmental conditions when applied without use of suitable carrier materials.
Aim: The study entailed synthesis of nanocarrier materials for biological control agents (BCAs) using Chitosan and silica nanocomposites.

_____

Corresponding author: E-mail: hwanyika@jkuat.ac.ke;

Site and Duration: The experiments were carried out at Jomo Kenyatta University of Agriculture and Technology for a period of two years June 2013 to June 2015.
Methodology: The experiments were conducted using a completely randomized design with three replications. Deacetylation, functionalization and immobilization of chitin on mesoporous silica nanoparticles (MSN) to form chitosan immobilized silica nanocomposites (CISNC) gel was done.
Results: This resulted in formation of chitosan nanoparticles and CISNC with crystallite sizes of 2.8 and 4.4 nm respectively. BCAs were adsorbed on CISNC gel. Characterization of the bio-nanocomposites showed that they had physisorption properties thus, ideal carriers for BCAs. CISNC gel had the highest significant ($P=.05$) sorption properties with 75% and 65% adsorption and desorption respectively of BCAs. Efficacy trials were done by *in vitro* pathogen inhibition and greenhouse bioassays using tomato seedlings. Adsorption of BCAs on CISNC gel significantly ($P=.05$) increased inhibition efficacy of BCAs on *R. solanacearum* from 50 to 70%. This was attributed to the antibacterial effect of the individual substances and the overall synergy acquired. Further, BCA-CISNC gel forms a film around root hairs, initiates fast wound healing mechanism and induce prophylactic effect on tomato seedlings challenged with *R. solanacearum* pathogen, decreasing wilting incidences from 45 to 25%. Additionally, BCA-CISNC complex significantly ($P=.05$) increased tomato seed germination from 70 to 80% and growth rate from 12 to 15% due to enhanced water utilization efficiency, induced phytohormones and nutritional benefit. BCAs also aided faster nutrient release, absorption and utilization by tomato plants.
Conclusion: Therefore, adsorption of bacterial, fungal and phage biocontrol agents on CISNC gel, a complex hitherto not reported to have been used in *R. solanacearum* disease control, enhanced microbial efficacy against the pathogen and increased tomato productivity.

1. INTRODUCTION

Tomato is one of the most widely cultivated crops in the world [1]. In Kenya, production is mainly affected by pests and diseases, postharvest losses and soil degradation [2]. Bacterial wilt of tomato is one of the most serious soil borne pathogens in Kenya that limits the production of tomato and other solanaceae crops [2]. The disease is caused by *Ralstonia solanacearum which is a severe* soil borne pathogen. The pathogen is favoured by high temperature and humidity, which are the ideal greenhouse conditions [3]. Thus, huge losses of yield and income are incurred by the greenhouse tomato farmers [2]. It has been previously reported that the pathogen's persistence and variability, makes its control difficult [4]. Chemical use has been attributed to environmental pollution and results in pathogen mutations [5].

Biological control has the potential of controlling the pathogen [6]. A number of soil bacteria and plant growth promoting rhizobacteria are currently being investigated for their role in the control of *R. solanacearum*. Various biological antagonists such as *Bacillus subtilis*, *Bacillus thuringiensis, Pseudomonas fluorescence, Trichoderma viridae* and *Glomus mosseae* are able to produce volatile compounds and different lytic enzymes that are known to suppress the pathogen. However, commercial utilization of the BCAs has not been realized [7]. This is due to their inability to adapt to newly introduced environment and at times harsh abiotic conditions that render them ineffective. In order to increase the efficacy of the BCAs, compatible carrier materials like clay, silica and polymers have been tested. *In vitro* tests of the BCAs and composites have shown positive results [8].

Bacteriophages are other biological antagonists of *R. solanacearum.* These phages are viruses that specifically target and reproduce within bacterial cells, using the host DNA for replication, translation and transcription, leading to eventual death of the infected cell. The host specificity nature of phages offers a suitable technology for viral therapy in the control of bacterial pathogens. Research has demonstrated their usefulness for treating bacterial infections in livestock, plants, aqua-cultured fish and humans [9]. The advantage of viral therapy over other disease control methods is the ability to target particular hosts, evolve with the host and the unlikeliness to elicit pathogen resistance [10,11].

Application of microbial antagonists and viral therapy for bacterial disease control is an attractive and a likely antidote for the pathogen.

However, commercial success in agricultural practices will depend on developing improved delivery systems with consistent positive results. The field efficacy of the antagonists is constrained by their short shelf life, inability to adapt and lack of virulence to the pathogen when applied in a harsh environment, hence the need for an appropriate carrier material in delivery of the biological antagonist through soil and plant system [12].

This necessitated exploration of various materials as carriers for the BCAs. Polymeric microparticles and nanoparticles are suitable carriers; however, nanoparticles are mostly preferred due to their large surface area for attachment and a shorter diffusional path for the substrates [13]. Nano-structured carriers were therefore, utilized in this study. The choice of the nano-materials for adsorbing the BCAs was based on safety of the material, sorption properties, anti-bacterial properties and ability to form complex nanocomposites. The above properties; that is; biocompatibility, nontoxicity and antimicrobial effects informed the choice of chitosan and mesoporous silica nanoparticles as carrier materials for the BCAs [13].

Chitosan was synthesized from chitin as the polymer is readily available. Chitin is the second most abundant natural polysaccharide after cellulose [14]. Effect of chitin as an antimicrobial agent was hampered by its low solubility in most non-toxic solvents and inertness [15]. The limitation was overcome by activation of chitin to chitosan (Fig. 1) through deacetylation using concentrated alkaline solution. Deacetylation of chitin made it soluble in acidic conditions due to the free protonable amino groups present in the

D-glucosamine units. Chitosan possess antagonistic effects on soil pathogens and potential to deliver biological control antagonists due to ease of functionalization. Chitosan was then functionalized further to form chitosan nanoparticles which increased the surface area for adsorption and the degree of deacetylation [16].

In order to prevent rapid degradation after administration, increase sorption properties and efficacy, the biocompatible polymer coating was immobilized on silica nanoparticles through physisorption (Fig. 2). Nano-silica was preferred due to its inherent antimicrobial characteristic, enhancement of host plant resistance, large surface area due to large gallery spaces that appear like "honey comb" structures when observed under transmission electron microscope [17,18]. Therefore, the objective of this study was to investigate the effect of biological control antagonists adsorbed on chitosan immobilized silica nanocomposite on *R. solanacearum* and growth of tomato seedlings. Hybrid tomato varieties of Anna and Chonto were used in this study due to their high yield, adaptability to greenhouse conditions and susceptibility to *R. solanacearum* wilt [19].

2. EXPERIMENTAL DETAILS

2.1 Experimental Site and Layout

The experiments were carried out in Jomo Kenyatta University of Agriculture and Technology elevation of 1600 metres above sea level (m ASAL) at the department of Horticulture in phytotechnology laboratory and greenhouse for *in vitro* and field tests respectively.
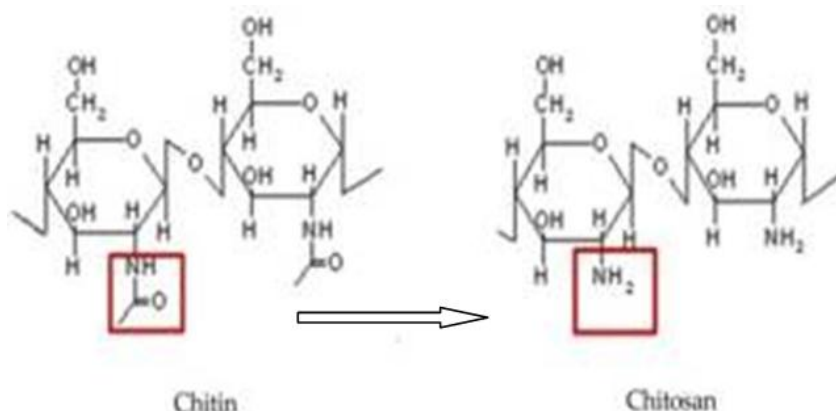

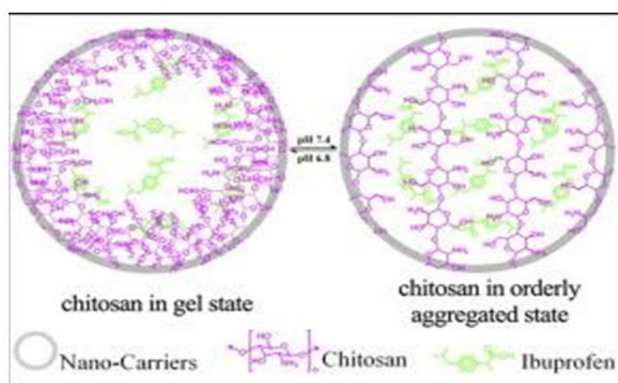**Fig. 1. Structural formula of chitin and chitosan [20]**

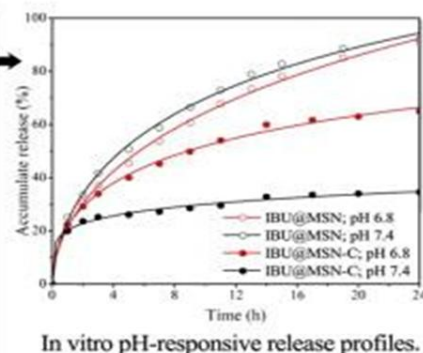**Fig. 2. Structure of chitosan immobilized silica gel [18]**

Fig. 3. Release of biotic substances at different pH levels [18]

All reagents were at least analytical grade. Sodium hydroxide (NaOH) pellets, acetic acid, glutaraldehyde (25%), L-cysteine, hydrogen peroxide (H_2O_2), phosphate buffered saline (PBS), tri-poly phosphate (TPP), potassium dichromate ($K_2Cr_2O_{7)}$, sulpuric acid, hydrochloric acid, orthophosphoric acid, diphenyl amine indicator, ammonium ferrous sulphate, copper sulphate, mesoporous silica nanoparticles (MSN), chlorox, tetrazolium chloride (TZC) were obtained from Sigma Aldrich, UK. PCR kit, primers forward–GAA CGC CAA CGG TGC GAA CT-, and reverse –GGC GGC CTT CAG GGA GGT C- for *R. solanacearum*, forward–GTG CCT GCC TCC AAA ACG ACT- and reverse–GAC GCC ACC CGA TCC CGC ATC CCT C- for *R. solanacearum* phage, agarose gel, ethidium bromide, nutrient agar (NA), nutrient broth and potato dextrose agar (PDA), were obtained from Bioneer Corporation, hybrid tomato seeds (Anna and Chonto) were purchased from De ruiters, chitin (99%) was acquired from Laborex, *Bacillus subtilis* and *Trichoderma viridae* from Real IPM while *Glomus mosseae (mycorrhiza)* and effective micro-organisms were obtained from Juanco SPS Ltd Kenya. Cocopeat and planting trays were obtained from Amiran (K) Ltd.

2.2 Preparation of Chitosan (CHT) and Chitosan Nanoparticles (CHTNP)

Chitin was ground using a milling machine to obtain fine powder which was filtered on a 0.1 mm mesh to obtain very fine powder. It was then autoclaved at 121°C for 15 min after the autoclave attained a constant temperature of 121°C. It was then divided into 6 equal portions of 100 g each. The samples were treated separately with 20, 40, 60, 80 and 100% (w/v) NaOH solutions. The samples were then placed

in an oven at 100°C for 4 hr for deacetylation (removal of acetyl groups from the polymer) to take place. Modified centrifuge-ionic gelation method was used for synthesizing chitosan nanoparticles by dissolving chitosan in 1 M acetic acid to obtain a concentration of 1 g/10 ml, 1 ml hydrogen peroxide and 10 ml TPP (10% w/v) were added followed by centrifuging at 6000 rpm for 10 min to form chitosan nanoparticles. The sample was then characterized using Shimadzu Fourier transform infra red (FTIR) spectrometer and Rigaku X-ray powder diffractomer (XRD) [21].

2.3 Determination of Deacetylation

The degree of deacetylation was determined by estimation of carbon and nitrogen contents in chitin and chitosan. The ratio of carbon and nitrogen were used to determine deacetylation. Equations i, ii and iii were used as shown below.

2.3.1 Percentage of carbon

This was done by determination of percent (%) carbon in the chitin and chitosan based on the Walkey-Black chromic acid wet oxidation method. The amount of carbon was estimated as percentage using the following equation;

$$C = \frac{(B-T*0.3*V*0.75)}{WB} \qquad (1)$$

Where; C=carbon percentage, B=amount of titrant consumed by blank, T= amount of titrant consumed by sample, W= weight of the sample, V= volume of $K_2Cr_2O_{7,}$ 0.3= constant, 0.75= assumption that the sample had 75% carbon [22].

2.3.2 Percentage of nitrogen

Percentage nitrogen in chitin and chitosan were determined using the Kjeldahl method.

$$N(\%) = \frac{(VHCl * NHCl) - (VBK * NNaOH) - (VNaOH * NNaOH)}{1.4007W/100} \quad (2)$$

where;

$VHCl$ – Volume (ml) of standard HCl pipetted into titrating flask for sample
$NHCl$ - Normality of HCl
VBK – Volume (ml) of standard $NaOH$ needed to titrate 1 ml standard HCl minus B
B – Volume (ml) of standard $NaOH$ needed to titrate reagent blank carried through the method and distilled into 1 ml standard HCl
$NNaOH$ - Normality of $NaOH$
$VNaOH$ – Volume (ml) of standard $NaOH$ needed to titrate the sample
1.4007- milliequivalent weight of nitrogen *100
W - Weight of the sample in grams [22].

2.4 Calculation of Degree of Deacetylation (DDA)

The % C and N in chitosan were used to determine the DDA in chitin using the Kasaai equation;

$$DDA \% = \frac{(6.857) - \left(\frac{C}{N}\right)}{1.7148} \quad (3)$$

Where; DDA-degree of deacetylation, 6.857-Constant, C-Percentage carbon, N-Percentage nitrogen, 1.7148-Constant [23].

2.5 Preparation of Chitosan Immobilized Silica Nanocomposites (CISNC)

A 500 mg sample of MSN was dispersed in 100 ml phosphate buffered saline (PBS) to form a partial solution. Solubilized chitosan nanoparticles (50 ml) were added to 100 ml of MSN suspension. The mixture was vortexed for 2 min and placed in a vibratory shaker for 2 hr then magnetic stirrer for 2 hr. Excess suspension of MSN that was not adsorbed in the chitosan gel matrix was poured carefully and disposed. The gelly substance left behind was the chitosan-silica nanocomposites. A drop of 25% glutaraldehyde was added to the chitosan nanoparticles-MSN mixture using a syringe. The mixture was vortexed and placed on a magnetic stirrer for 1 hr [8,24]. This resulted in the formation of chitosan immobilized silica nanocomposites gel denoted CISNC.

2.6 Determination of Crystallite Sizes of Chitosan Nanoparticles and Nanocomposites

The CISNC was dried at 50°C for 48 hr to obtain a plaque that was used for XRD characterization. The crystallite sizes were determined using Scherrer equation;

$$D = \frac{K\lambda}{\beta Cos\theta} \quad (4)$$

Where, D is the crystallite size λ is wavelength of X-ray, β is full width and half maxima value, θ is Bragg's angle [23].

2.7 Isolation of *R. solanacearum*

Diseased hybrid tomato plant materials were obtained from a greenhouse in Thika, Kiambu County. The area is an endemic zone of *R. solanacearum* pathogen with reported wilt incidences of over 70% [2]. The plants were thoroughly washed to remove dirt. They were then dipped in 1% chlorox for sterilization. The lower stem was cut into small pieces of 5cm cross-sectionally and cut longitudinally then placed in a 1 L beaker containing distilled water to allow flow of bacterial exudates. The obtained bacteria were cultured in a sterilized growth chamber for 48 hr at 32°C on nutrient-TZC agar contained in a petridish. The colonies observed using a hand lens and light microscope. Pathogenicity of the pathogen was determined by appearance of whitish colonies with pink margins in cultured pathogen under light microscope [5].

2.7.1 Isolation of *R. solanacearum* phage

A viral suspension was prepared from soil samples collected from the *R. solanacearum* infested greenhouses. The soil was sieved through a 1 mm sieve to obtain fine particles. 50 g of the soil, adjusted to 40% moisture holding capacity with sterile distilled water was placed in 500 ml conical flasks. Each flask was seeded for 48 hr with cultures of the host bacteria (2.000 optical density *R. solanacearum* inoculum). The enriched soil samples were suspended in phosphate buffered saline (PBS). The mixture was centrifuged in 50 ml plastic tubes at 2000 revolutions per minute (rpm) for 10 min. The supernatant was aseptically transferred to a sterile 15 ml tube without disturbing the pellet. A viral suspension was prepared by aseptically filtering the supernatant through a 0.8 μm pore

sized cellulose filter to remove particulates, followed by filtration through a 0.45 µm pore sized filter to remove bacterial cells and cellular debris. Three drops of 2.000 optical density *R. solanacearum* inoculum were added to 1 ml of the isolated phage and cultured on nutrient broth for 48 hr at 32°C. The phage was cultured in a sterilized growth chamber for 48 hr at 32°C on 20 ml nutrient TZC agar. The plaques on the cultured pathogen confirmed positive isolation of the phage [25].

2.7.2 Molecular detection of isolated microbes

Suspensions of isolated and cultured *R. solacearum* and *R. solanacearum*-phage cells were prepared using distilled water. The suspensions were standardized to an optical density (O.D) of 2.000 observed at 600 nm on the Shimadzu Ultra violet visible (Uv-vis) spectrophotometer. The suspensions were used for DNA extraction using the CTAB extraction method. CTAB extraction buffer (500 µl) comprising of (100 Mm Tris Hcl [pH 8], 2% [w/v] CTAB, 50 Mm EDTA, 0.7 M NaCl, 0.17% [v/v] ß-mecarptoethanol and 1% [w/v] PVP), pre-warmed to 65°C, two glass beads added and the mixture placed in miller at a frequency of 30/sec for 5 min. Samples were incubated at 65°C for 30 min in a water bath. Chloroform (500 µl) - isoamyl choloroform) (24:1 v/v) was added and the two phases were mixed several times by vortexing. The tubes were centrifuged at 14,000 rpm for 10 min at room temperature in a microfuge. The supernatant was removed and transferred into new 1.5 Eppendorf tube. 10 µl of RNase A was added and mixed by vortexing. The samples were then incubated in a water bath at 37°C for 30 min. Centrifuging and addition of RNase A were repeated to ensure that all RNA was separated from the DNA. An equal volume of cold isopropanol (pre-chilled in a -20°C freezer) was added mixed and incubated at -20°C in a freezer for 30 min. The samples were then centrifuged at 14000 rpm for 10 min at room temperature in a microfuge and supernatant removed. 500 µl of 70% ethanol (at room temperature) was added to the tube containing DNA, centrifuged at 14000 rpm for 5 min and the supernatant carefully poured off. The 70% ethanol wash was repeated once, the supernatant carefully poured off and the DNA pellet dried for 60 min by leaving the tube open. Low salt TE buffer (100 µl) was added to the dried pellet. The pellet was dissolved by incubating at 37°C in a water bath for 30 min. 1.0

µl of DNA was used for electrophoresis on Agarose gel to determine presence of the DNA. The DNA was then stored at -20°C [26].

2.7.2.1 DNA amplification

The polymerase chain reaction (PCR) was done using touchdown procedures as described by Korbie and Mattick [26]. The primers used were a 20 mer forward primer –GAA CGC CAA CGG TGC GAA CT-, and reverse –GGC GGC CTT CAG GGA GGT C- for *R. solanacearum* and 21 mer forward primer–GTG CCT GCC TCC AAA ACG ACT- and reverse –GAC GCC ACC CGA TCC CGC ATC CCT C- for *R. solanacearum* phage. The amplification reactions were performed in 25 µl volumes in thin-walled PCR tubes after optimization in a Programmable Thermal Controller (PTC-100), programmed for an initial 5 cycles of 30 sec at 94°C, 3 min at 48°C, annealing at 58°C for 1 min, extension for 1 min at 72°C, followed by 10 and 15 cycles at the same timing and conditions. The samples were cooled up to 4°C, subjected to electrophoresis on a 1.5% agarose gel in 1X TAE buffer (40 mM Tris acetate and 1.0 mM EDTA). The obtained ladders were interpreted using base pair amplicons to detect the microbes [27,28].

2.7.3 Culturing of biocontrol antagonists (BCAs)

The microbial products (*B. subtilis*, *T. viridae*, *G. mosseae*) and effective micro-organisms were centrifuged at 2000 rpm for 10 min to obtain a supernatant containing the cellular suspension. Five drops of the supernatant were cultured on the respective media contained in petridishes to confirm viability. The NA was used to culture bacterial microbes while PDA was used to culture fungal microbes. The cultured microbes in petridishes were tightly sealed to prevent cross-infection then placed in a growth chamber for 48 hr and 96 hr at 32°C and 28°C for the bacterial and fungal microbes respectively. After multiplication of the microbes, each microbe was carefully collected using a wire loop, placed in 10 ml distilled water and mixed for 5 min on a vortex mixer [12].

2.8 Adsorption of Antagonistic Microbes onto CISNC

Aliquot volumes of 50 ml for *B. subtilis*, *G. mosseae*, *T. viridae*, effective micro-organisms and *R. Solanacearum* phage were

adjusted to 2.000 optical density (O.D) at 600 nm using a Uv-vis spectrophotometer. The standardized microbes were then added separately to each sample of 100 ml CISNC, placed on a rotary mixer (130 rpm) for 2 hr and on a magnetic stirrer for 2 hr to allow for adsorption. The concentration of microbes in the supernatant after adsorption was determined using Uv-vis spectrophotometer to determine adsorption efficiency. The desorption efficiency was determined after addition of 1 g/100 ml L-cysteine to the BCA-nanocomposite gel and centrifuging at 6000 rpm for 10 min. The concentration of microbes in the supernatant was determined using the Uv-vis spectrometer [8]. Adsorption of BCAs on CISNC gel was also observed under the Nixon compound microscope.

2.8.1 *In vitro* tests

R. solanacearum pathogen was standardized to 2.000 O.D using Uv-vis spectrophotometer then cultured on nutrient agar contained in a petridish. Effect of the BCAs-nanocomposites on the pathogen was done in vitro as follows;

The experiment was laid out in a completely randomized design (CRD) with 20 treatments and 4 replications inside a growth chamber at 32°C for 96 hr. Filter papers adsorbed with bio-nanocomposite were placed on particular pathogen colonies to determine inhibition of *R. solanacearum.* Inhibition was measured in mm^2 using a 30 cm ruler and a magnifying glass. Inhibition was estimated as;

$$\text{Inhibition} = \frac{\text{Colony size after inhibition}}{\text{Colony size before inhibition}} \times 100 (5) \text{ [29].}$$

2.9 Seed Treatment

Tomato seeds (50) per treatment were soaked in 1 mg/1 ml of particular bio-nanocomposites (BCA-CISNC gel) for 4 hr followed by drying for 1 hr in a growth chamber at 25°C. They were then challenge treated with a 2.000 O.D *R. solanacearum* suspension for 30 min and left to dry overnight in a sterile lamina flow chamber. Seeds treated with acetic acid and distilled water served as controls [3].

2.9.1 Media preparation

Cocopeat block (5 kg) was soaked in tap water to fragment and form a friable planting material. It was then washed with running water until a pH of 6.5 was obtained. Compound fertilizer NPK 17.17.17 (50 g), trace elements (5 g poly feed) and 100 ml of nutrient broth mixed thoroughly with prepared cocopeat to provide tomato seeds and micro-organisms with necessary starter nutrients respectively. Cocopeat was then placed on 60 hole- plastic trays.

2.9.2 Sowing of seeds, estimation of: Germination percentage, chlorophyll content, growth rates and wilt incidences

Treated hybrid tomato seeds from two varieties (Anna and Chonto) were sown in plastic trays. The seeds were closely monitored to determine germination, growth vigour and wilt incidences. The chlorophyll content in the leaves was also determined 8 weeks after planting. The germination rate was estimated as a percentage of the seeds emerging against the number of seeds sown per treatment. The relative chlorophyll content in the leaves was measured using the Chlorophyll Meter SPAD 505 (Minolta, Japan). The meter measured leaf transmittance at 600 nm. The measurement entailed sampling any three top leaves from one plant per treatment. The measurements were taken at different points and averages used to determine the chlorophyll content. The plant vigour or growth rate was taken by measuring the shoot growth using a tape measure after every 10 days. The change in shoot length was taken to represent the growth rate. Wilting incidence was based on symptoms of wilting leaves. This was monitored daily for 90 days after planting.

Disease severity was assessed using modified Champoiseau et al. [3] wilting scale of 1–5. Where 1-healthy; 2-mild wilting of one or two leaves during day time; 3-wilting of all but the top two leaves during the day time; 4-wilting of all leaves during the day; or 5-wilting of all leaves during daytime and no recovery when cool early in the morning or late in the evening.

Wilting incidence was calculated using the formula:

$$\frac{(5A + 4B + 3C + 2D + E)}{1.75 N} \tag{6}$$

where, A= number of plants on scale 5; B= number of plants on scale 4; C= number of plants on scale 3; D= number of plants on scale 2; E= number of plants on scale 1; N=total number of plants. From the scale, the lower incidence level the better the control measure [30].

Each experiment consisted of 20 plants per treatment. The plants were arranged in a growth chamber in a completely randomized design (CRD). The plants were grown in the growth chamber for 21 days then transplanted in plastic pots containing cocopeat in the greenhouse. Another set of tomato plants treatments were sown directly on well prepared ground inside the greenhouse. During transplanting, the seedlings were inoculated with the respective bio-nanocomposite by soaking in a 10 % solution for 15 min and inoculating with the *R. solanacearum* pathogen for 5 min. The transplanted plants were arranged in a C.R.D with three replicates [28].

2.10 Data Analysis

The data on pathogen colony inhibition, germination rates, growth rates and wilt incidences were subjected to analysis of variance (ANOVA) and means compared by protected Fischer's Least Significant Difference (LSD $_{0.05}$). Origin-pro statistical package and genstat version 7.0 were used for data analysis [31].

3. RESULTS AND DISCUSSION

3.1 Deacetylation of Chitin

Carbon and nitrogen content in chitin and chitosan were used to estimate the degree of deacetylation. The quantity of carbon and nitrogen decreased with deacetylation of chitin to form chitosan (Table 1).

The degree of deacetylation (DDA) was affected by concentration of sodium hydroxide. The findings are corroborated by Fig. 4.

Reduction of carbon and nitrogen contents in chitin after deacetylation (Table 1) was attributed to the loss of acetyl groups resulting in a polar and soluble chitosan (Fig. 4) [32]. The positive charge was a result of the amino group formed after deacetylation (Fig. 1). When percentage DDA was plotted against the NaOH concentration, a linear fit was obtained, an indication that concentration of NaOH affected deacetylation. This was confirmed by the fact that, the highest deacetylation of 90.9% was obtained when a concentration of 100% w/v of NaOH was used. This was in agreement with the Tsaih and Chen [33] observation that, as the concentration of alkaline increased, deacetylation increased proportionally. The resultant linear fit

of deacetylation had a strong coefficient of determination (R^2) value of 0.939 (Fig. 4) a confirmation that DDA of chitin is directly proportion to the concentration of alkaline media used.

In addition to the linear graph, FTIR spectra for the deacetylated chitin showed reduced peaks attributed to loss of acetyl groups. The most pronounced peak reduction being on the 90.9% deacetylated chitin (Fig. 5). Diffractogram variances were noted on the XRD output for chitin and its derivatives (Fig. 6). This confirmed attainment of deacetylation [34]. It was also found out that, deacetylation of chitin at low sodium hydroxide concentration below 60% yielded less than 50% chitosan. This observation had been postulated by Cao et al. [9] that, effective deacetylation of chitin occurs at high concentration of alkali as the temperature, time and pH remained constant [35].

Table 1. Content of carbon and nitrogen in acetylated and deacetylated chitin

Substance	Content	
	Carbon %	Nitrogen %
Chitin*	41.5	5.9
Chitin**	38.7	5.3
Chitin***	35.1	4.9
Chitin****	33.8	4.3
Chitin*****	32.1	3.9
Chitin******	30.3	3.6

*-As purchased, **-20% NaOH treated, ***-40% NaOH treated, ****-60% NaOH treated, *****-80% NaOH treated,******-100% NaOH treated

Solubility of chitosan in dilute acids is always associated with D-glucosamine units. This compound result after deacetylation of chitin. Hence, pure chitosan is composed entirely of the compound and is highly soluble in dilute acids. On the contrary, pure chitin is composed of N-acetyl-D-glucosamine units [36]. In most cases, only impure chitin and chitosan are obtained. The compounds are therefore, comprised of N-acetyl, D-glucosamine and D-glucosamine units at varying degrees respectively. Chitin used in this study comprised of 10.2% D-glucosamine units while the purest form of chitosan obtained was 90.9% (Table 1).

3.2 Characterization of Deacetylated Chitin

There were spectral changes of chitin after deacetylation in the formation of chitosan (Fig. 5).

The FTIR spectrum of chitin was slightly different from that of chitosan with DDA above 60%. The differences in spectra were observed in form of shifts in bands. This was attributed to loss of acetyl groups in chitosan (Fig. 5). However, since a 100 % deacetylation was not attained (Table 1), there were notable similarities in the spectra of chitin and chitosan. Occurrence of glucosamine units were attributed to spectral similarities between chitin and chitosan involved in this study [37]. The two, had absorption peaks around 3444.6 and 3435.0 cm^{-1} for chitin and chitosan respectively. These peaks indicated the presence of -OH stretching and amine N-H symmetric vibrations. The slight shift to the left marked reduced intensity of –OH stretching and N-H vibrations between chitin and chitosan. The bands at 1070.4 cm^{-1} and 1028 cm^{-1} for the chitin and chitosan respectively are due to the -C-O groups stretching vibrations. The C-O groups in chitosan were depressed due to deacetylation. The absorption band at 1413 cm^{-1} characterized stretching vibration of amino group in chitosan. Also, peaks between 1070.4-1028 cm^{-1} and 530-540 cm^{-1} indicated the presence of saccharide structure of chitin and chitosan respectively due to the varying C-O groups [38]. This confirmed the polysaccharide nature of chitin and its derivatives used in the study.

The defractrogram of chitin was changed after deacetylation (Fig. 6).

The XRD diffractogram of chitin was observed to be partly crystalline while chitosan had a clearer crystalline structure. The difference in crystallinity between the two compounds was attributed to

deacetylation (Fig. 6). Higher concentration of sodium hydroxide resulted in pronounced peaks. The chitin spectra showed characteristic peaks at 2-theta 9.25 and 19.05 but were shifted to 9.45, 20.5 and 31.89 suggesting formation of inter and intra-molecular hydrogen bonds in the presence of free amino groups. The shifts were attributed to formation of amine groups and cleavage of intra-molecular hydrogen bond of chitosan [21]. There was systematic reduction in d spacing from chitin to chitosan confirming that chemical change had occurred between the compounds. The process of deacetylation was necessary in synthesizing a soluble and reactive compound since pure chitin is neutral in charge and almost inert. Solubility of chitosan is attributed to the presence of protonable amino group developed after deacetylation [39].

3.3 Characterization of Chitosan Nanoparticle and Chitosan Immobilized Silica Nanocomposite (CISNC)

There was change in the crystallite sizes of chitosan nanoparticle when CISNC was formed. Chitosan nanoparticle had a smaller crystallite size than the nanocomposite (Table 2).

The XRD difractograms indicated notable differences of, d-spacing, 2-theta and Full width and half maxima values between chitin, chitosan, chitosan nanoparticles and CISNC (Fig. 7). The crystallite sizes were derived from the XRD difractograms using the Scherrer equation (4).
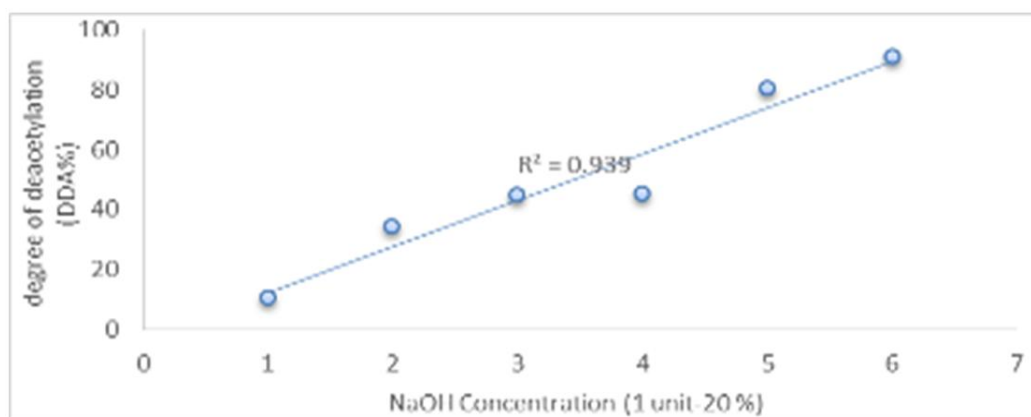

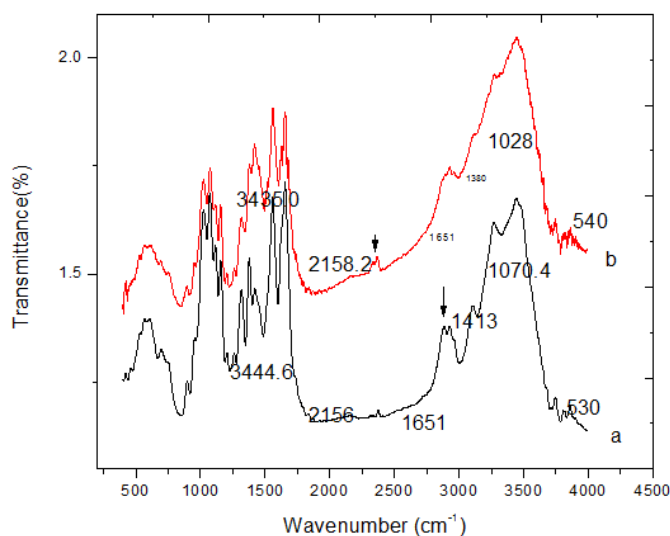**Fig. 4. Linear fit for deacetylation of chitin using sodium hydroxide**

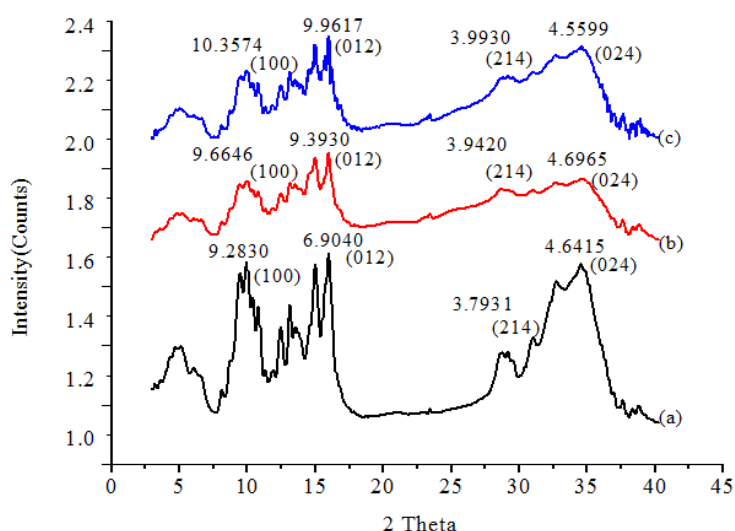**Fig. 5. FTIR spectra of a) chitin and b) chitosan**

Fig. 6. XRD diffractograms for (a) Chitin, (b) Chitosan and (c) Chitosan-nanoparticle

Table 2. Crystallite size of chitosan nanoparticles and chitosan immobilized silica nanocomposites

Substance	Crystallite size (nm)	Method
Chitosan nanoparticle	2.8	X-ray powder diffraction
CISNC	4.4	

There was a slight increase in the size of the chitosan nanoparticles from 2.8 nm to 4.4 nm in the synthesized CISNC (Table 2). The change in crystallite size was attributed to immobilization of MSN into the chitosan nanoparticles matrix. The nanocomposites aggregated together forming larger particles thus the increased crystallite sizes. Addition of glutaraldehyde which is a good cross-linking agent enhanced adsorption of MSN on the chitosan nanoparticles gel. The nanocomposite acquired the sorption properties of the two nanoparticles making the nanocomposite superior [16].

Chitosan diffractogram showed characteristic peaks at 2-theta 9.45 and 19.05 but were shifted to 9.46, 20.5 and 31.89 and 9.46, 20.5, 31.89 and 45.69 for chitosan nanoparticle and nanocomposite respectively. This illustrated formation of physical molecular bonds in
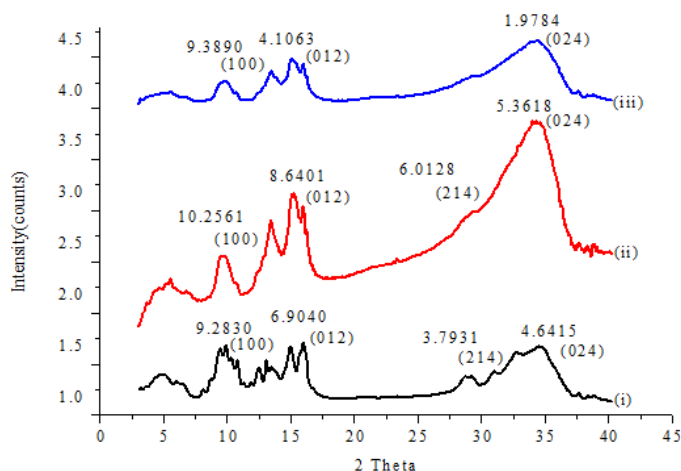
Fig. 7. X-Ray Diffractograms of; (i) Chitin, (ii) Chitosan nanoparticle and (iii) CISNC

nanoparticles and nanocomposites. The physical bonds in the nanocomposite were the basis of using it as a carrier material, due to ease of disintegration when pH and moisture contents are varied. In addition, the d-spacing of chitosan nanoparticles and nanocomposites of chitosan and silica varied with notable reduction in interlayer distances. The peaks sensitive to crystallinity decreased and/or disappeared in the spectrum of chitosan and chitosan nanoparticles due to reduced crystallinity (Fig. 7). Formation of chitosan nanoparticle resulted in a fairly new product with a slightly small d-spacing than chitosan, immobilization of chitosan nanoparticles on silica nanoparticles was a physical process thus the small difference in the d spacing. The d value however, reduced after formation of chitosan nanoparticles showing that the nanoparticle layers have a smaller d-spacing than chitosan. Addition of MSN and glutaraldehyde were responsible for the marked differences between chitosan nanoparticle and its nanocomposite product [40]. There was no notable difference of d-spacing in the chitosan-silica nanocomposite and chitosan nanoparticle. This meant that MSN occupied the interlayer spaces within the chitosan nanoparticles matrix (Figs. 6 and 7). Immobilization of MSN on chitosan nanoparticle resulted in amplified peaks, exemplifying successful capping and formation of a composite [21].

Synthesis of chitosan nanoparticles and CISNC was also notable after characterization using FTIR spectrometry (Fig. 8).

FTIR spectrometry indicated a peak at 1413 cm^{-1} assigned to stretching vibrations of amino groups in chitosan that shifted to 1415.7 cm^{-1} in the nanoparticle and then changed to 1380 cm^{-1} in the CISNC after adsorption/impregnation of silica nanoparticles on chitosan nanoparticles. The broad peak at 1028 cm^{-1} in chitosan became less intense in chitosan nanoparticle by shifting to 1076.2 cm^{-1} showing that C-O stretching vibrations reduced in the chitosan nanoparticle spectrum. The vibration band at 3431.1 cm^{-1} denoted increased intensity of chitosan nanoparticle confirming that vibrations of N-H increases as the particle sizes decrease (Fig. 8). The absorption band at 3431.1 cm^{-1} shifted to 3445 cm^{-1}, the shift indicated possible overlapping and stretching of hydrogen bounded –OH and -NH_2. The characteristic band at 2841 cm^{-1} was attributed to presence of glutaraldehyde in the compound. This is because of the typical -CH bond around 2900 cm^{-1} in glutaraldehyde. Thus the new band at 2841 cm^{-1} in the nanocomposite confirmed cross-linking. There were distinct spectral shifts in chitosan nanoparticle from 1415.7, 1076.2 and 565.1 cm^{-1} to 1383, 1082 and 505 cm^{-1} associated with formation of new hydrogen bonds between molecules in the nanocomposite [15,20].

3.4 Detection of Isolated Microbes

The isolated *R. solanacearum* pathogen and phage were confirmed after culturing by morphological characterization on compound microscope (Plate 1).

The *R. solanacearum* pathogen was confirmed by observing the pink coloration after addition of TZC on the culturing media [20], while phage was visible from the *R. solanacearum* plaques (Kalpage and Costa [11]. The plaques indicated

lysis which results after colonization of the pathogen by phage.

In addition to microscopic observations, PCR detection was employed as the ultimate confirmation test (Plate 2).

The *R. solanacearum* phage and *R. solanacearum* bacteria were detected at 300 base pairs (bp) and 600 bp respectively (Plate 2) [41]. The method clearly confirmed the presence of the two bioagents because molecular characterization results in over 99% accuracy in detection of organisms. Touchdown PCR procedure was preferred as RT-PCR had limitations in determination of the optimal temperature for clear display of PCR ladders [26].

3.5 Sorption Properties of Biological Antagonists on CISNC

CISNC gel had the highest adsorption activity on BCAs while chitin had the least. Adsorption

efficiencies of microbial antagonists on CISNC are represented in Fig. 9. The nanocomposites were observed under a compound microscope (Plate 3).

There was increased adsorption of BCAs when chitosan was converted to chitosan nanoparticles. The adsorption rate increased several folds when a composite of chitosan nanoparticles and MSN were used (Fig. 9). The enhanced adsorption was attributed to large gallery spaces in MSN and gel properties of the chitosan. Deacetylation of chitin to chitosan therefore, enhanced adsorption of BCAs because chitosan has free amino groups creating a charged environment that attract the charged microbial membranes [38]. Immobilization of MSN on the chitosan nanoparticle membranes resulted in formation of Si-OH bonds with polar characteristics enhancing further adsorption [41].

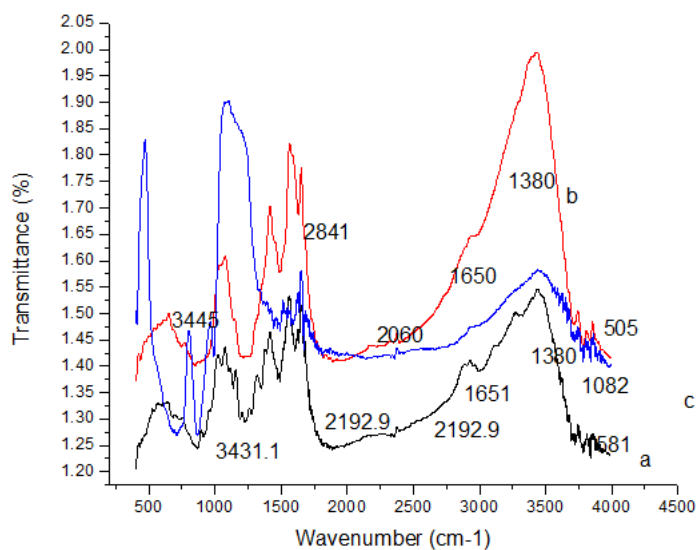Desorption of microbial antagonists was enhanced when L-cysteine was added to the CISNC gel (Fig. 10).

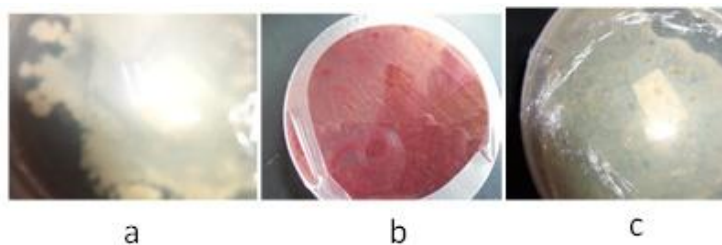**Fig. 8. FTIR patterns for a) chitosan nanoparticle b) CISNC and c) MSN**

Plate 1. Images of; a) *R. solanacearum* cultured on NA b) *R. solanacearum* cultured on TZC-NA c) Plaques formed in cultured *R. solanacearum* cells due to lysis by the phage

The suitability of a carrier material is in its ability to desorb the substrate (s) on reaching the target site. There was therefore need for desorption of the BCAs from the CISNC carrier as an indication that the microbes will be released while inside the tomato plant system. The BCA should be discharged from the nanocomposite and synergistically with the dissociated nanoparticles destroy the pathogen. This role was achieved by enhancing the vitality of the BCA using a carrier material that has good sorption properties. The change of conditions in plants which can cause desorption include; pH, pressure and moisture level. Addition of glutaraldehyde ensured successful adsorption of the BCAs on to CISNC gel by increasing stability of the nanocomposite through cross-linking. This activity reduces leakages during delivery to the target [42]. Conversely, addition of L-cysteine in the BCA-CISNC matrix enhanced desorption of the BCAs by overcoming cross-linking effect associated with the glutaraldehyde and electrostatic membranes attraction between the microbes, silica and chitosan charges [12].
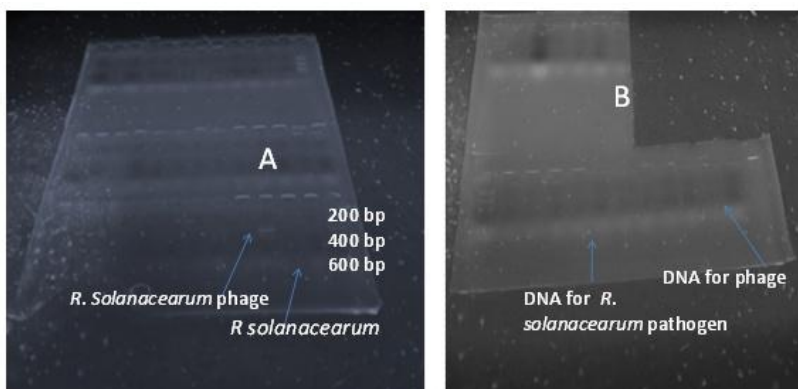

Plate 2. Electrophoresis images; A- Amplified DNA of *R. solanacearum* and phage, B-Isolated DNA from *R. solanacearum* bacteria and phage respectively
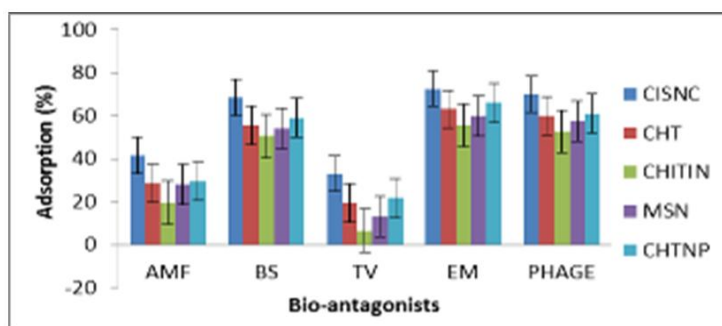

Fig. 9. Microbial antagonists cells adsorbed on different substances
Means significant at L.S.D $_{0.05}$ (F-test) ^{l}-standard error bar
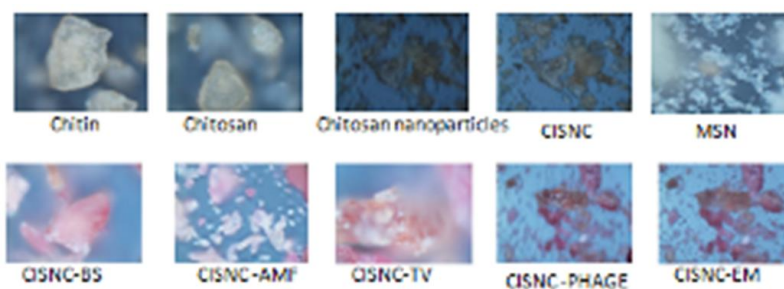

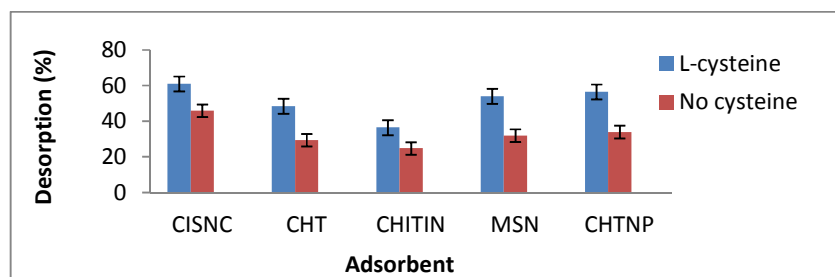**Plate 3. Images of nanocomposites from a compound microscope**

Fig. 10. Optical densities of microbial antagonists' suspensions after desorption from the different substances
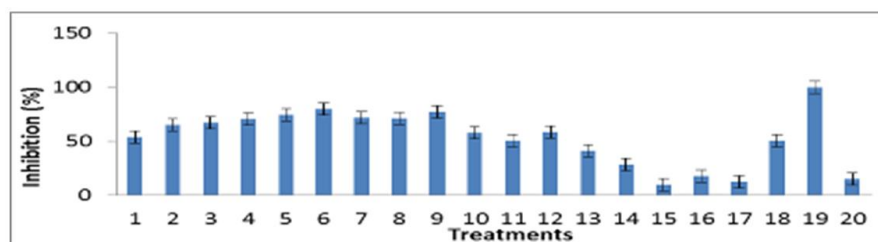*Means significant at L.S.D $_{0.05}$ (F-test) ᴵ-standard error bar*

Fig. 11. *In vitro* inhibition of *R. solanacearum* growth on different substances
Means significant at L.S.D $_{0.05}$ (F-test) ᴵ-standard error bar

Key
Treatments
1. Chitin 2. Chitosan 3. Chitosan nanoparticle (Chtnp) 4. Chitosan immobilized silica nanocomposites (CISNC) 5. CISNC-BS 6. CISNC-EM 7. CISNC-TV 8. CISNC-AMF 9. CISNC-PHAGE 10. Phage 11. Bacillus subtilis (BS) 12. Effective micro-organisms (EM) 13. Trichoderma viridae (TV) 14. Glomus mosseae (AMF) 15.Ralstonia solanacearum (RS) 16. Acetic acid 17. Mesoporous silica nanoparticles (MSN) 18. Glutaraldehyde 19. L-Cysteine 20. Distilled water 21. 10%TPP solution
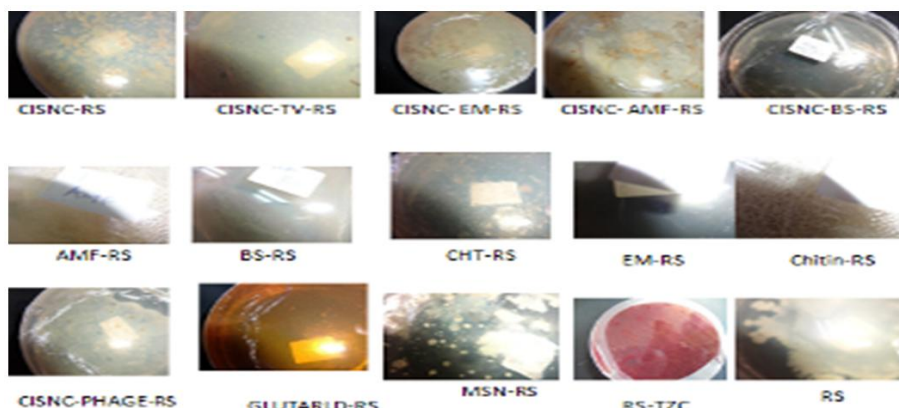

Plate 4. Images of cultured *R. solanacearum* on CISNC and bio-nanocomposites

3.6 Efficacy of the BCA-CISNC Complex on *R. solanacearum*, Tomato Wilt and Growth

3.6.1 *In vitro* inhibition of *R. solanacearum*

BCAs adsorbed on CISNC gel had the highest pathogen inhibition effect (Fig. 11). The observations are also corroborated in Plate 4.

Deacetylation of chitin to chitosan, functionalization of chitosan to chitosan nanoparticles and immobilization of chitosan nanoparticle on MSN, to form CISNC gel, significantly (*P=.05*) increased *R. solanacearum* pathogen growth *in vitro*. For instance, application of chitin on *R. solanacearum* cultured on nutrient agar caused a colony inhibition of 53.9%. The bacterial inhibition was attributed to

the fact that, the near neutral charged chitin possessed antibacterial effect due to the presence of minimal glucosamine units. Further, chitosan with 90.9% DDA depicted a 65.3% inhibition. The enhanced inhibition was attributed to positive charges of amino groups that disrupted cellular functions of the charged bacterial membrane, thus destroying the cells (Fig. 11 and Plate 4). Interactions between positively charged chitosan molecules and negatively charged residues of bacterial cell surface also played an important role in the inhibitory effect of gram negative bacterial pathogen. The inhibition was also attributed to direct toxicity, chelation of nutrients and minerals from the pathogen. In addition, the biopolymer properties of chitosan engulf pathogens causing suffocation [18]. Additionally, chitosan stimulate microbial degradation of *R. solanacearum* pathogen in a manner resembling the application of a hyper-parasite. Chitosan has also been found to inhibit other plant pathogens like *Pseudomonas syringe* resulting in reduced crop losses [41].

Formation of chitosan with a high DDA was paramount in this study. The DDA in chitosan has an effect on the positive charge density which impacts on polycationic effect. This had been observed by Christian et al. [13] and Taraskiewicz et al. [33], where chitosan with higher DDA conferred stronger antibacterial activity than moderate DDA against *Staphylococcus aureus* (*S. aureus*) at acidic pH. Development of low molecular weight chitosan nanoparticles, enhanced the *R. solanacearum* pathogen inhibition significantly (*P=.05*). The nanochitosan had an inhibition of 67.2%, attributed to ease of penetration of the nanoparticles through the pathogen membranes, causing rapid cell destruction and death. The observation was in agreement with Liu et al. [43] findings, where bactericidal activity of chitosan correlated strongly with the molecular weight of chitosan. An increase in molecular weight of chitosan reduced effect on *E. coli.* The current study was in agreement with the previously reported work by Jaworska et al. [44], where formation of chitosan nanoparticles corresponded with a lower molecular weight. The low molecular weight increased ease of penetration thus enhancing efficacy against pathogens. The low molecular weight chitosan nanoparticles had a higher concentration of positively charged amino groups which adsorbed more pathogen antagonist cells. The inhibitory effect on *R. solanacearum* pathogen by chitin

and chitosan derivatives was associated with the ability of the low molecular weight and water-soluble glucosamine penetrating the bacterial cell wall and combining with DNA inhibiting synthesis of mRNA and transcription of DNA. According to Taraskiewicz et al. [33], higher molecular weight and soluble chitosan interacts with cell surface altering the cell permeability. The interaction cause cellular leakage or formation of an impermeable layer around the cell. This activity blocks transportation of essential solutes into the cell. Experiments conducted on *E. coli* treated with both high molecular weight and low molecular weight chitosan, revealed that, some microbial species display significant differences in the mode of action depending on different dimensions of chitosan particles. The results are consistent with the idea that chitosan kill bacteria through an interfacial inhibitory effect that occurs on the surface of the microspheres. Transmission electron microscope image of *E. coli* cell showed appearance of leaking outlets and empty cell envelops [17]. Immobilizing cross-linked chitosan with nanosilica, enhanced the efficacy of the nanocomposite by increasing inhibition of *R. solanacearum* pathogen colonies from 67.2% to 70.4% for the chitosan nanoparticles and nanocomposite respectively. The increased efficacy was attributed to the synergy of the nanocomposite since MSN alone reduced the *R. solanacearum* colonies to 50.4%.

Adsorption of BCAs on CISNC gel increased inhibition of the pathogen significantly (*P=.05*). This was attributed to the inhibitory effect of individual members and the resultant synergy. For instance, the antibacterial effect of effective micro-organisms (58.4%) was enhanced to (79.6%) after adsorption on CISNC gel (Fig. 9). Adsorption of BCAs was made possible by the fact that, most microbes have a net charge on their membranes, which allow their adsorption to polar materials. This formed the basis for adsorption of bacteria, fungi and viruses achieved in the study. The negatively charged *R. solanacearum* pathogen was therefore, strongly attached to the inhibiting BCA-nanocomposite hence destroying the pathogen [8].

Cao et al. [9] and Choong and Wolfang [37] reported that, glutaraldehyde increases entrapment efficiency by up to 73%. Entrapment ensured that the BCAs were released on reaching the target site. Thus, an increase in efficacy depicted by higher inhibition of the pathogen. On the other hand, L-cysteine aided desorption of BCA from CISNC gel and resulted

in adsorption of the gram negative *R. solanacearum,* due to its higher affinity for the positive charge in the nanocomposite. This resulted in destruction of the weakened and immobilized pathogen by both the BCAs and CISNC [32].

3.6.2 Effect of BCA-CISNC and *R. solanacearum* on tomato seed germination

BCA-CISNC complex caused the highest effect on germination rates of tomato seeds while glutaraldehyde inhibited germination of tomato seeds (Fig. 12).

3.6.2.1 Germination rates of treated tomato seeds

Seeds treated with chitin, its derivatives and BCAs showed a significant (*P=.05*) germination rate compared to the controls. Chitin treated seeds had a germination rate of 80.3%, chitosan treated seeds had a germination rate of 83.6% while CISNC gel treatment increased germination rate to 86.4% (Fig. 12). The variation in germination was attributed to the ability of the chitin derivatives to form a semi-permeable film on the seed surface which maintained seed moisture in the growing media promoting seed germination [45]. Chitosan contained in the CISNC gel increased seed germination in tomato seeds since it caused a decline in malonydialdehyde content, a compound that inhibits germination. Chitosan also altered the relative permeability of the plasmalemma, increased concentration of soluble sugars and enzymes such as proline, peroxidase, polyphenol oxidase and catalase. In addition, it acts as a permeation enhancer by opening epithelial tight junctions allowing free entry of water, nutrients and air. The mechanism underlying this effect is based on the interaction of positively charged chitosan and the cell membrane resulting in a re-organisation of the tight junction-associated proteins. Algam et al. [29] indicated that, chitosan has an amino group (-NH$_2$) that makes it hygroscopic. When it gets in contact with water, the amino group is protonated turning it into ammonia (-NH$_3$) which confers more hygroscopicity to the chitosan molecule making the seed or plant trap more moisture. Furthermore, Chitosan increases the water utilization efficiency of plants, increase mineral uptake and stimulate growth rate.

The enhanced germination in CISNC gel treatments can also be attributed to the role of silica nanoparticles. The material has a large surface area and surface reactivity. It has the ability of penetrating cell walls acting as a media for transport intracellularly. The increased permeability enhances water and air uptake hence accelerated germination [8]. Treatment of tomato seeds with MSN increased germination and growth vigour in tomato seedlings. The MSN treated seeds had a germination percentage of 78.3% and a growth rate of 11.9% while distilled water which served as one of the controls had a germination and growth rates of 71.5% and 10.9 respectively (Figs. 12 and 13). Increased silica concentration leads to higher availability of phosphorus in most crops. This is because, the anions formed by silicates competes with phosphates for the same sorption sites [46]. Phosphorus is one of the macro nutrient elements that promote growth and development in plants. In related studies, Moussa [47] observed that Si increased seed germination in wheat and maize. It also corrects acidity in the growing media thus enhanced growth in acidic media. Furthermore, silica affects seed weight and heavier seeds have better developed embryo due to higher amount of food reserves with better germination ability.

Adsorption of BCAs on CISNC gel increased tomato seeds germination significantly (*P=.05*). For instance, effective micro-organisms adsorbed on CISNC gel had the highest germination rate of 90.7% from 82.7%. All biocontrol agents had a significant (*P=.05*) effect on germination when compared to the controls. According to Roberts et al. [48], BCAs' synthesize plant hormones like auxins and cytokinins which solubilize soil phosphorus and enhance soil porosity. The synthesized phytohormones triggers faster germination, reduce the mean germination index and result in more vigorous plants. Other studies have shown that application of *Paernibacillus polymyxa* increased tomato seed germination by 44%. This qualifies BCAs as germination stimulants. There was an important observation in this study, although glutaraldehyde had the highest antibacterial effect on *R. solanacearum*, it reduced germination capacity to 61%. This was attributed to its oily characteristic that inhibited imbibition rendering the testa slightly impervious. However, its effect as a germination inhibitor was alleviated when used in cross-linking of CISNC in minute quantities (0.2%).

3.6.3 Effect of bio-antagonists nanocomposite on chlorophyll content

Treatment of tomato seedlings with CISNC increased the chlorophyll content significantly (*P=.05*) (Table 3).

3.6.3.1 Induced chlorophyll content

The application of chitosan derivatives and/or MSN resulted in tomato seedlings plants with significantly (*P=.05*) higher chlorophyll content compared to the controls (Table 3). The increased chlorophyll is caused by accelerated biochemical activities in the tomato seedlings triggered by the glucosamine units in chitosan and silicates in MSN. Confirming the above observation, Dzung et al. [49] reported that spraying of coffee seedlings with chitosan solution increased the content of chlorophyll and

carotenoids in leaves by 15% for plants grown in the field and by 46–73% for plants grown in the greenhouses.

Inclusion of Silica in the chitosan gel matrix was also attributed to the increased chlorophyll activity. These results are consistent with the finding of Cao et al. [9] who, found out that, leaf senescence of sugarcane (*Saccharum officinarum* L.) could be delayed with silica application. Effects of silica deposited in leaves improved chlorophyll efficiency in rice, barely, wheat and sugarcane [50].

3.6.4 Effect of BCA-CISNC and *R. solanacearum* on tomato plants growth

BCAs adsorbed on CISNC stimulated the highest growth rates in tomato seedlings (Fig. 13). The growth rates are also displayed in Plate 5.
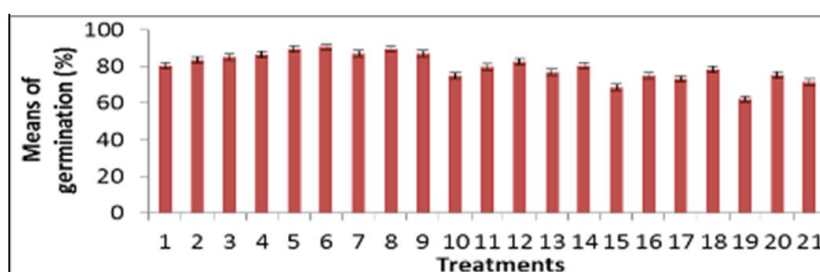

Fig. 12. Germination rates of tomato seeds treated with BCA-CISNC
Means significant at L.S.D $_{0.05}$ (F-test) ⁱ-standard error bar

Table 3. Means of chlorophyll content in tomato seedlings treatments

Treatment	Means	R-square	C.V %	F-value	F-prob
1.	30.7ab	0.76463	27.78	123.449	1.689 E-13
2.	38.6a				
3.	41.4a				
4.	35.6a				
5.	32.2a				
6.	37.6a				
7.	34.0a				
8.	35.3a				
9.	33.0a				
10.	26.5b				
11.	28.8b				
12.	29.6b				
13.	29.3b				
14.	29.7b				
15.	20.8b				
16.	22.0b				
17.	27.9b				
18.	30.8a				
19.	25.7b				
20.	26.4b				

ANOVA Means followed by similar letters are not significantly different. LSD $_{0.05}$

3.6.4.1 Growth rate of treated tomato seedlings

Tomato Seedlings treated with chitin, its derivatives and BCAs showed significant (*P=.05*) plant vigour inferred from the shoot growth. Seedlings treated with CISNC gel adsorbed with effective micro-organisms had the highest growth rate (14.2%). The enhanced growth rate was attributed to the role of BCAs as biostimulants and provision of nutrients in the rhizosphere. Chitosan played a role in stimulating growth of beneficial microbes due to high carbon content in the polymer. The activated microbes accelerated decomposition of organic matter into inorganic forms. The BCAs in addition, enhanced root system development enabling the plants to absorb more nutrients from the soil. Chitosan also caused chelation of nutrients and acted as a fertilizer due to the high nitrogen and carbon contents. Cao et al. [9] found out that, chitosan contains oligosaccharides that act on plants as phytohormones which regulates morphogenesis and development. It also promotes plant growth through increasing availability and uptake of water and essential nutrients by adjusting osmotic pressure. Chitosan treatment increased chlorophyll content in tomato plants (Table 3), hence, high net photosynthesis [16,49]. Guan et al. [45] found out that, chitosan enhanced germination index, reduced mean germination time, increased shoot height, root length, shoot and dry weights. It also promoted the growth of microbial species with antagonistic action against pathogens.

High molecular weight chitosan stimulated faster growth than low molecular weight chitosan nanoparticles (Fig. 12 and plate 5). This was consistent with Iriti et al. [51] that, long polymer or high molecular weight chitosan has stronger positive charge which presents a greater capacity as a chelating agent in soil than the lower molecular weight type. The high molecular chitosan also contained higher amounts of elements such as silica, carbon and nitrogen. MSN which is essentially silica had impressive plant vigour effect, attributed to stress reduction, physiological roles and increased chlorophyll in
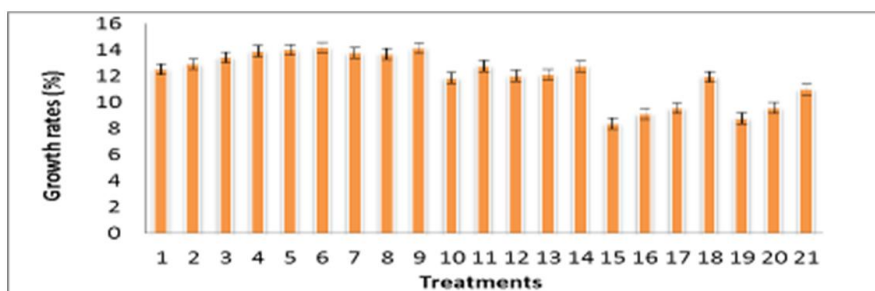

Fig. 13. Growth rates of tomato seedlings treated with BCA-CISNC
Means significant at L.S.D $_{0.05}$ (F-test) ^{I}-standard error bar

Key
a-CISNC
B-Microbes
c-Control
d-CISNC-Microbes

Plate 5. Images of tomato seedlings treated with bionanocomposites

plants. Hence, inclusion of MSN in the nanocomposite fortified effect of CISNC gel [5,52].

3.7 Effect of BCA-CISNC and *R. solanacearum* on Tomato

Tomato seedlings treated with BCA-CISNC complex particularly the effective micro-organisms and phages had the least wilt incidences (Fig. 14).

3.7.1 Biological control agents in the control of *R. solanacearum* wilt in tomato seedlings

BCAs significantly (*P=.05*) reduced wilting in tomato seedlings. Effective micro-organisms for instance, had the highest effect of reducing the tomato seedlings wilt incidence (0.205) (Fig. 13). The high efficacy of effective micro-organisms was attributed to innate synergy between the microbial composites which is comprised of; photosynthetic bacteria, lactobacillus and the actinomycetes fungi [6,7,30,53]. The *R. solanacerum*-phage had a significant (*P=.05*) effect on wilt suppression in tomato seedlings (0.4). Viral therapy is an effective control strategy due to specificity of the virus to the pathogen. The control is also sustainable due to the fact that, it can easily be isolated from the soil. Phages are persistent and are easily translocated in tomato plants infected by the pathogen, particularly the xylem vessels. The problem with phage as a reliable therapy mechanism is in timing when to apply the phage [54]. Thus the need to apply phages before pathogen infestation [55]. Moreover, efficacy of the phage was greatly reduced when applied without use of carriers. The current study had consistent results with Iriarte et al. [42], where bacteriophage completely controlled the *R. solanacearum* pathogen *In vitro*.

B. subtilis reduced wilt incidences significantly (*P=.05*). The ability of *B. subtilis* to produce volatile compounds and different lytic enzymes such as protease and cell wall degrading enzymes such chitinase and glucanase was attributed to the increased resistance in tomato seedlings. Additionally, *T. viridae* reduced wilting in tomato seedlings. The reduction was attributed to the fact that, *Trichoderma spp.* especially *T. viridae* and *T. hazarnium* are able to stimulate production of secondary metabolites in plants [6]. This play a major role in suppressing pathogens directly or indirectly by promoting

plant growth and enhancing plant disease resistance as well as the lytic enzymes. Moreover, *T. viridae* inhibits growth of pathogens by competition for nutrients and for space as it grows more rapidly. Trichoderma species are also known to be pathogenic to most plant pathogens. In some circumstances however, they also depress plants acting as plant pathogens. This depressing effect of Trichoderma was not observed in this study [4,7,53]. Finally, *G. mossesase* significantly (*P=.05*) reduced wilt incidence. This is because, mycorrhiza increases phenols in plants. Phenols are known to have antimicrobial effect on most pathogens. Another method employed by the fungi to reduce wilting in plants is by colonizing the root hairs, denying soil borne pathogens entry in to the plant system. It also reduces *R. solanacearum* populations in the rhizosphere of plants by denying the pathogen access to nutrients and space for replication. BCAs are therefore able to reduce wilt incidences by antagonizing pathogens and eliciting systemic protection in plants [6].

Complementarily, adsorption of the BCAs on the synthesized CISNC gel reduced bacterial wilt significantly (*P=.05*). The efficacy of the BCA-CISNC complex was several folds higher than the non-adsorbed microbes. The reduced wilt incidence was attributed to positive synergy of all constituent substances. The nanocomposite played a major role in ensuring the vitality of the microbial antagonists during storage and after application [56]. It was construed that the nanocomposite delivered the BCAs precisely to the target site and protected them from harsh environmental conditions enhancing their efficacy. In addition, the CISNC gel ensured sustained release of the microbes trapped in its matrix [12,57]. However, BCAs are more likely to be preventive than therapeutic on disease pathogens. Hence, their potential should be harnessed by seed priming and/or pre-treatment before transplanting [29].

3.7.2 Chitosan in the control of *R. solanacearum* wilt

Chitosan and its derivatives reduced wilting in tomato plants significantly (*P=.05*). When applied alone, it reduced the wilt incidence to a scale of 0.425 (Fig. 13). The wilt reduction was attributed to induction and accumulation phytoalexins. Chitosan also contains oligosaccharides which induce proteinase inhibitors in tomato leaves that cause an increase in host plant
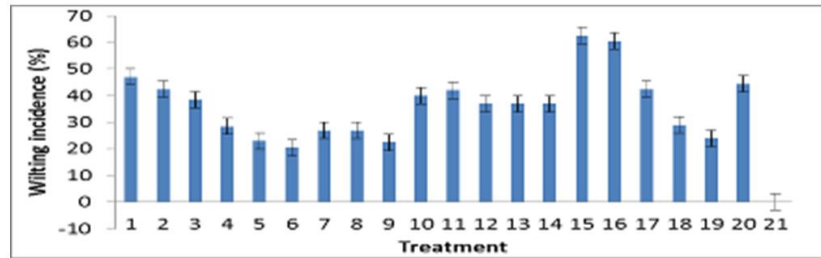
Fig. 14. *R. solanacearum* wilt incidences in tomato seedlings treated with BCA-CISNC
Means significant at L.S.D $_{0.05}$ (F-test) ᶦ-standard error bar, Fvalue (58.73) > F prob (3.17)

resistance. Chitosan has also been found to increase lignification in wheat plants. Increased lignin accumulation makes pathogen penetration in plants difficult by fortifying the cell wall [58]; [59]. Chitosan is also known to elicit many plant defense responses by activating pathogenesis-related gene functions such as chitinases, chitokanase and β-glucanases [60].

Directly, chitosan stimulates microbial degradation of pathogens in a way resembling the application of a hyper-parasite. Additionally, due to high polysaccharides, it stimulates the activity of beneficial micro-organisms upsetting pathogenic microbial equilibrium in the rhizosphere [61]. El-Hadrami et al. [62] reported that, chitosan is easily degraded producing pathogen repellents like ammonia which pre-dispose pathogens to the emboldened biological antagonists making the adsorbed miro-organisms more efficacious in controlling the pathogen. Combining BCAs and chitosan in the control of bacterial wilt as done in this study had not been reported hitherto.

3.7.3 Silica in the control of *R. solanacearum* wilt

Mesoporous Silica Nanoparticles (MSN) reduced wilt incidence significantly (*P=.05*) to 0.425 when compared to the control (Fig. 13). The reduction of wilt caused by *R. solanacearum* pathogen was attributed to the fact that silica augments resistance in tomato seedlings. This is because assimilated silica in plants inhibits fungal and bacterial diseases by physically inhibiting penetration of the epidermis through lignification of the membranes [63]. Silica is a precursor in the synthesis of lignin. Hence, improves seed coat resistance, decreases seed susceptibility to mechanical damage and metabolite leaching. In contrast to the above observation, Datnoff et al. [60] found out that silica did not significantly (*P=.05*) improve a susceptible cultivar resistance. However, Jian [64] proved that application of

silica led to activation of pathogenesis-related proteins such as catalase, peroxidase, polyphenol oxidase, glucanase, chitinase in a pathogen infected plant. The proteins are associated with in increased plant resistance to pathogens. This was in agreement with the current study where tomato seeds and seedlings treated with MSN and its derivatives were more resistant to *R. solanacearum* pathogen.

Formation of a chitosan-MSN composite increased the role of chitosan manifold causing significant difference (*P=.05*) in tomato seedlings wilting incidences treated with MSN and chitosan-MSN nanocomposite. The nanocomposite also had better sorption properties than MSN. This was attributed to the increased active sites for reaction due to the gel forming properties of the composite. According to Mandal et al. [59], induced lignification and antimicrobial biochemicals, could have played an important role in host plant resistance of tomato plants in this study.

4. CONCLUSION

Concentration of alkali used affects the degree of deacetylation in chitin. Chitosan with high DDA formed the basic building block for the highly efficacious bio-nanocomposites. The bio-nanocomposite enhanced bacterial wilt resistance, seed germination and growth rate in tomato. Therefore, formation of bio-nanocomposites in this study has opened a new front in plant pathology. It is recommended that biocontrol agents be applied using chitosan-silica nanocomposite carriers to enhance their efficacy.

COMPETING INTERESTS

Authors have declared that no competing interests exist.

REFERENCES

1. Islam M, Kim Y, Hong S, Baek J, Kim I, Kang H. Effects of cultural methods on quality and postharvest physiology of cherry tomato. J. Agricultural, Life and Environmental Sciences. 2013;25(3):15-19.
2. Fintrac Inc., USAID-KHDP. Kenya Horticultural Development Program October 2003-March 2009 Final Report; 2009
3. Champoiseau P, Allen J, Momol T. Description and strategies for best management of *Ralstonia solanacearum* Race 3 biovar 2 as a casuse of bacterial wilt of tomato. Proceedings of the 24th Annual Tomato Disease Workshop held on November. 3-5, State College, Pennsylvania. 2009;1-35.
4. Agrios G. Plant pathology. 5th edn, Academic press, NY, USA, ISBN. 13-9780120445653. 2005;922-924.
5. Jeong Y, Kim J, Kang Y, Lee S, Hwang I. Genetic diversity and distribution of Korean isolates of *R. solanacearum*. J. Plant Disease. 2007;91:1277-1287.
6. Nguyen M, Ranamukhaarachchi S. Soil-borne antagonists for biological control of bacterial wilt disease caused by *Ralstonia solanacearum* in tomato and capsicum. J. Plant Pathology. 2010;92(2):385-395.
7. Pal K, Mc Spadden B. Biological control of plant pathogens. Plant Health Instr. 2006; 1117-02.
8. Kubata M, Matsui M, Chiku H, Kasashima N, Shimojoh M, Sakaguchil K. Cell adsorption and selective desorption for separation of microbial cells by using chitosan immobilized silica. J. Appl. Environ Microbial. 2005;71(12):8895-8902.
9. Cao W, Jing D, Li J, Gong Y, Zhao N, Zhang X. Effects of the degree of deacetylation on the physicochemical properties and Schwann cell affinity of chitosan films. J. Biomater. Appl. 2005;20: 157-177.
10. Fujiwara A, Fujisawa M, Hamasaki R, Kawasaki T, Fujie M, Yamada T. Biocontrol of *R. solanacearum* by treatment with lytic bacteriophages. J. Appl. Environ Microbiol. 2011;77:4155-62.
11. Jones J. Bacteriophages for plant disease control. J. Annu. Rev. Phytopathol. 2007; 45:245–262.
12. Spadaro D, Gullun M. Improving the efficacy of biocontrol agents against soil borne pathogens. J. Crop. Prot. 2005;24: 601-613.
13. Christian P, Kammer F, Baalousha P. Nanoparticles: Structure, properties, preparation and behavior in environmental media. J. Ecotoxicology. 2008;17(5):326-343.
14. Kumar M. A review of chitin and chitosan applications. React. Funct. Polym. 2012; 46:1-27.
15. Zouhour L, Salah S, Saloua S, Amor E. Extraction and characterization of chitin and chitosan from crustacean by-products-biological and physicochemical properties. African J. of Biotech. 2010;10(4):640-647.
16. Li L, Deng J, Liu L, Xin L. Synthesis and characterization of chitosan-zinc oxide nanocomposite membranes. J. Carbohyd. Res. 2010;345:994-998.
17. Freier T, Koh H, Kazazian K, Shoichet M. Controlling cell adhesion and degradation of chitosan films by N-acetylation. J. Biomaterials. 2005;26:5872-5872.
18. Rodrigo S, Vieira M, Beppu M. "Interaction of natural and cross-linked chitosan membranes with Hg (II) ions Colloids and Surfaces. J. Physicochem. Eng. Aspects. 2006;279:196–207.
19. De Ruiters. A grower's handbook. Monsatto Hybrid seeds; 2002.
20. Wang S, Shen L,Tong Y, Chen L, Phang L, Lim P, Liu T. Biopolymer chitosan/montmorillonite nanocomposites; preparation and characterization. Polymer degradation and stability. J. Chem. 2005; 90:123-131.
21. Ogawa K, Yui T. Structure and function of chitosan. 3. Crystallinity of partially N-acetylated chitosans. J. Biosci. Biotech. Bioch. 1993;57:1466-1469.
22. Jaber Y, Mehanna N, Sultan S. Determination of ammonium and organic bound nitrogen by inductively coupled plasma emission spectroscopy. Talanta. 2009;78(4-5):1298-1302.
23. Cullity B, Stock S. Elements of X-Ray Diffraction, 3rd Ed., Prentice-Hall Inc. 2001;167-171.
24. Zhang Z, Chen D, Chen L. Preparation of two different serials of chitosan. J. Dong Hua Univ. (Eng. Ed.). 2002;19:36-39.

25. Yamada T. A jumbo phage infecting the phytopathogen *R. solanacearum* defines a new lineage of the Myoviridae family. J. Virology. 2007;398:135-147.

26. Korbie J, Mattick S. Touchdown PCR for increased specificity and sensitivity in PCR amplification. J. Nat Protoc. 2008;3(9): 1452-6.

27. Fujiwara A, Kawasaki T, Usami S, Fujie M, Yamada T. Genomic characterization of *R. solanacearum* phage and its related pro-phage. J. Bacteriol. 2008;190:143-156.

28. Wydra K, Semrau J. Phenotypic and molecular characterization of the interaction of antagonistic bacteria with *R. solanacearum* causing tomato bacterial wilt. In: Wolfgang Zeller, Cornelia Ulrich (eds.). 1st International Symposium on Biological Control of Bacterial Plant diseases, Darmstadt, Germany 2005. 2006;112-118.

29. Algam S, Xie G, Li B, Yu S, Su T, Larsen L. Effects of paenibacillus strains and chitosan on plant growth promotion and control of *R. solanacearum* wilt in tomato. J. Plant Pathol. 2010;92(3).

30. Ramesh R, Phadke G. Rhizosphere and endophytic bacteria for the suppression of eggplant wilt caused by *Ralstonia solanacearum*. J. Crop Protection. 2012; 37:35–41.

31. Hinkelmann K, Kempthorne O. Design and Analysis of Experiments. I and II (Second ed.). Wiley 470-38551-7; 2008.

32. Chatelet C, Damour O, Domard A. Influence of the degree of acetylation on some biological properties of chitosan films. J. Biomaterials. 2001;22:261-268.

33. Taraskiewicz A, Fila G, Grinholc M, Nakonieczna J. Innovative strategies to overcome biofilm resistance. J. Biomed Research International; 2013.

34. Harish P, Kittur F, Tharanathan R. Solid state structure of chitosan prepared under different N-deacetylating conditions. J. Carbohydr. Polym. 2002;50:27-33.

35. Knaul J, Kasaai M, Bui V, Creber K. Characterization of deacetylated chitosan and chitosan molecular weight review. Can. J. Chem. 1998;76:1699-1706.

36. Domszy J, Roberts G. Evaluation of infrared spectroscopic techniques for analyzing chitosan. Makromol. J. Chem. 1985;186:1671-1677.

37. Choong J, Wolfgang H. Chemical modification of chitosan and equilibrium study for mercury ion removal. J. Water Research. 2003;37(19):4770–4780.

38. Jolanta K, Malgorzata C, Zbignew K, Anna B, Krysztof B, Jorg Tand Piotr S. Application of spectroscopic methods for structural analysis of chitin and chitosan. Marine Drugs. 2010;8:1570-1577.

39. Nasri A, Zaki M, Leonardis D, Ungphaiboon S, Sansongsak P, Rimoli G, Trelli N. Chitosan/TPP and Chitosan/TPP-hyaluronic acid nanoparticles. Systematic optimization of the preparative process and preliminary biological evaluation. J. Pharm. Res. 2009;26:1918-1930.

40. Kim C, Nair S, Kim J, Kwak H, Grate W, Kim H, Gu B. Preparation of biocatalytic nanofibers with high activity and stability via enzyme aggregate coating on polymer fibers. J. Nanotech. 2005;16:3882-3888.

41. Fleming C, Wingender J. The biofilm matrix nature. Rev. Microbiol. 2010;8:623-633.

42. Iriarte F, Obradovic A, Wernsing M, Jackson L, Balogh B, Hong J, Momol M, Jones J, Vallad G. Soil-based systemic delivery and phyllosphere *in vivo* propagation of bacteriophages. Bacteriophage. 2012;2(4):215-224.

43. Liu H, Du Y, Wang S, Sun L. Chitosan kills bacteria through cell membrane damage. Int J. Food Microbial. 2004;95:147-155.

44. Jaworska M, Sakurai K, Gaudon P, Guibal E. Influence of chitosan characteristics on polymer properties: I: Crystallographic properties. J. Polym. Int. 2003;52:198-205.

45. Guan J, Wang, Shao X. Seed priming with chitosan improves maize germination and seedling growth in relation to physiological changes under low temperature stress. J. Zhejiang Univascie B. 2009;10:427-433.

46. Currie A, Perry C. Silica in plants: Biological, biochemical and chemical studies. J. Ann. Bot. 2007;100:1383–1389.

47. Moussa R. Influence of exogenous application of silica on physiological response of salt-stressed maize (*Zea mays* L.). International Journal of Biology Toronto. 2006;8(2):293-297.

48. Roberts D, Lohre S, Meyer S, Buyer J, Lewis J. Biocontrol agents applied individually and in combination or suppression of soil borne disease of cucumber. J. Crop Prot. 2005;24:141-155.

49. Dzung N, Minh H, Van Nguyen S. Study on chitosan nanoparticles on biophysical characteristics and growth of Robusta coffee in green house. J. Biocatalysis and

Agricultural Biotechnology. 2013;2(4):289–294.

50. Zeng X, Liang J, Tan Z. Effects of silicate on some photosynthetic characteristics of sugarcane leaves. J. Huazhong Agricultural University. 2007;26(3):330–334.

51. Iriti M, Pichi V, Maffi D, Faoro F. Chitosan in induced resistance: more chances than limits and vice versa? Proceedings of the 5th meeting of the IOBC working group induced resistance in plants against insects and diseases. J. Plant Disease. 2009;20-25.

52. Li F, Ma C. Effect of available silica in soil on cucumber seed germination and seedling growth metabolism. J. Acta Horticulturae Sinica, Beijing. 2002;29(5): 433-437.

53. Obradovic A, Jones J, Olson S, Jackson L, Balogh B. Integration of biological control agents and systemic acquired resistance against bacterial spot on Tomato. J. Plant Dis. 2005;89:712-6.

54. Balogh B, Jones J, Iriarte F, Momol M. Phage therapy for plant disease control. Curr. Pharm. Biotechnol. 2010;11:48–57.

55. Yamada T. Isolation and characterization of bacteriophages that infect the phytopathogen *R. solanacearum*. Microbial. 2007;153:2630-2639.

56. Se K, Niranjan R. Enzymatic production of biological activities of chitosan oligosaccharides. J. Carbohyd. Polym. 2005;62:357-368.

57. Xu Y, Du Y. Effect of molecular structure of chitosan on protein delivery properties of chitosan nanoparticles. Int. J. Pharm. 2003;250:215-226.

58. Ambrorabe E, Bonmort J, Fleurat-Lessard P, Roblin G. Early events induced by chitosan on plant cells. J. Exp Bot. 2008; 59:2317-2324.

59. Mandal S, Kar I, Mukherjee A, Acharya P. Elicitor induced defence responses in tomato against *R. solanacearum*. The Scientific World Journal; 2013.

60. Datnoff E, Deren W, Snyder H. Silica fertilization for disease management of rice in Florida. J. Crop Protection, Oxford. 1997;16(6):525-531.

61. Costa M, Silva S, Tavaria K, Pintado M. Study of the effects of chitosan upon streptococcus mutans adherence and biofilm formation. J. Anaerobe. 2013;20: 27-31.

62. El-Hadrami A, Adam L, El-Hadrami I, Daayf F. Chitosan in plant protection. J. Mar drugs. 2010;8(4):968-987.

63. Balakhina T, Borkowska A. Effects of silica on plant resistance to environmental stresses. J. International Agrophysics. 2013;27:225-232.

64. Jian F. Role of silica in enhancing the resistance of plants to biotic and abiotic stresses. J. Soil Science and Plant Nutrition. 2004;50:11-18.